Granular Matter 5, 75–83 © Springer-Verlag 2003
DOI 10.1007/s10035-003-0133-y

Dynamical properties of vibrofluidized granular mixtures

D. Paolotti, C. Cattuto, U. Marini Bettolo Marconi, A. Puglisi

Abstract Motivated by recent experiments we have carried out an Event Driven computer simulation of a diluted binary mixture of granular particles vertically vibrated in the presence of gravity. The simulations not only confirm that the kinetic energies of the two species are not equally distributed, as predicted by various theoretical models, but also seem to reproduce rather well the density and temperature profiles measured experimentally. Rotational degrees of freedom do not seem to play any important qualitative role. Instead, simulation shows the onset of a clustering instability along the horizontal direction.

Keywords Granular, Gravity, Mixture, Simulation, Equipartition

1 Introduction

The present keen interest in the dynamical properties of granular materials is motivated both by the challenge of understanding the complex processes involved and by the important practical applications in engineering, industry and technology [1]. These materials are peculiar in many respects and display several intriguing phenomena such as clustering [2], shear instability [3,4] and lack of energy equipartition, which make their behavior different from ordinary molecular fluids. The dissipation of kinetic energy during the inelastic collisions makes them special. The main motivation of the present paper stems from two recent experiments [5,6] which demonstrated that when a mixture constituted by two different species of grains is vibrated, each component attains its own "granular temperature", i.e. the average kinetic energy per particle does not take on the universal value fKT, where f is the number of degrees of freedom and K a constant, as it occurs in molecular gases. On the contrary, one observes that the ratio T_1/T_2 varies with the number fraction $x = N_1/N$ (where N_i is the number of grains of the i-th species and $N = N_1 + N_2$ is the total number), inelasticity parameters, particle sizes, masses and driving mechanism. Even in the absence of energy injection, the inelastic gas cools, but one observes that the temperature ratio asymptotically remains constant. On the other hand, it has been demonstrated that while the only relevant hydrodynamic field is the global temperature $T = xT_1 + (1 - x)T_2$ (because the partial temperatures T_1 and T_2 can be derived directly from T), transport properties depend on that ratio [7].

These are of course manifestations of the on-equilibrium nature of Granular systems, which can only be maintained stationary by a continuous energy feeding to compensate the energy losses due to the inelastic collisions and to friction.

A theoretical understanding of such a behavior of granular mixtures has been achieved in the case of homogeneous driving mechanisms by means of a combination of models and approximations including the pseudo-Maxwell inelastic gas and the Inelastic Hard Sphere model treated by means of the Boltzmann-Enskog equation. Both models have been studied analytically and numerically in the free cooling [8,9] and in the driven case [10–13]. Apart from the studies of ref [12,13] none of these investigations considered the role played by the gravitational field, by the strongly inhomogeneous boundary conditions employed in the experiments of refs. [5,6], by the roughness of the grains and by their rotational degrees of freedom. Moreover, there is still an open debate about the "best" energy feeding mechanism. Whereas theoreticians seem to favor a uniform thermal Gaussian bath, because it lends itself to a great deal of analytical work, a numerical computer experiment can test directly driving mechanisms

Received: 25 July 2002

D. Paolotti, U. Marini Bettolo Marconi
Dipartimento di Fisica,
Universitá di Camerino, 62032 Camerino, Italy

D. Paolotti, U. Marini Bettolo Marconi
Istituto Nazionale di Fisica della Materia,
Unità di Camerino, Camerino, Italy

C. Cattuto
Frontier Research System,
The Institute of Physical and Chemical Research (RIKEN),
Wako-shi, Saitama 351-0198, Japan and
Istituto Nazionale di Fisica della Materia,
Unità di Perugia

A. Puglisi (✉)
Dipartimento di Fisica Universitá "La Sapienza",
P. le A. Moro 2, 00198 Roma, Italy

A. Puglisi
Istituto Nazionale di Fisica della Materia,
Unità di Roma, Roma, Italy

This work was supported by Ministero dell'Istruzione, dell'Università e della Ricerca, Cofin 2001 Prot. 2001023848, by INFM and INFM *Center for Statistical Mechanics and Complexity* (SMC).

which are closer to those employed in a laboratory. The structure of the paper is the following: in section II we illustrate briefly the model, leaving the technical details to the appendix; in section III we discuss the results for the geometry of ref. [5]. In sec. IV we consider a different aspect ratio, namely a taller box, where gravity plays a more relevant role. Finally in sec. V we present our conclusions.

2 Model system

We decided to remain as close as possible to a commonly employed experimental set-up, by constraining the grains to move on a vertical rectangular domain of dimensions $L_x \times L_z$. The gravitational force acts along the negative z direction. The grains are assumed to be spherical and free to rotate about an axis normal to the xy plane. They receive energy by colliding with the horizontal walls, harmonically vibrating at frequency ν. The side walls instead are immobile and were chosen either smooth or rough according to the numerical experiment. When side walls are considered to be rough, they are assumed to have the same friction coefficient μ as the particles. The normal restitution coefficient with the walls is 1.

The collisional model adopted in the present paper corresponds to the one proposed by Walton [14]. It conserves both the linear and the angular momentum of a colliding pair, but allows energy to be dissipated by means of a normal restitution coefficient and a friction coefficient μ. The collision rule (given in detail in the appendix) takes into account a reduction of normal relative velocity of the two particles (V_n), a reduction of total tangential relative velocity (V_r) and an exchange of energy between those two degrees of freedom. The reduction of normal relative velocity is modeled by means of a non constant restitution coefficients $\alpha_{ij} \in [0,1]$, whose dependence by the relative velocity is of the form:

$$\alpha_{ij}(V_n) = \begin{cases} 1 - (1 - r_{ij}) \left(\frac{|V_n|}{v_0} \right)^{\frac{3}{4}} & \text{for } V_n < v_0 \\ r_{ij} & \text{for } V_n > v_0 \end{cases}$$

where i and j are the numbers indicating the species of the colliding particles, r_{ij} are constants related to the three types of colliding pairs, $v_0 \approx \sqrt{gd}$, where d is the average diameter of the particles and g the gravitational acceleration [15].

Simulated collisions are of two types: with sliding or sticking point of contact. When the following condition is satisfied (high relative tangential velocity), the collision happens in a sliding fashion, otherwise it is sticking:

$$\frac{|V_r|}{V_n} \geq \frac{l+1}{l} \mu (1 + \alpha_{ij}) \qquad (1)$$

where l is the dimensionless moment of inertia (equal to $1/2$ for disks), while μ is a static friction coefficient characterizing the surface roughness of particles, assumed equal to the dynamical friction coefficient. The full dynamics consists of inter-particle collisions, and wall-particle collisions. The trajectories between collision events are parabolic arcs due to the presence of the gravitational field.

An efficient Event Driven (ED) simulation code was employed to evolve the system [16].

The two species were chosen to be spheres of equal diameters $d = 0.16cm$, and unequal masses $m_1 = 1.58 \cdot 10^{-2} g$ and $m_2 = 5.21 \cdot 10^{-3} g$, respectively. The driving frequency was set to 50 Hz, the vibration amplitude $A = 3.5$ diameters so that the corresponding dimensionless acceleration $\Gamma = A\omega^2/g = 56$. These parameters correspond to the experimental conditions of Feitosa and Menon [5].

All the averages quantities reported in the following have been obtained by employing equally spaced data points separated by time intervals $\Delta t = 10^{-1}$ s in order to assure statistical independence of measures. We performed a number $n = 1.5 \cdot 10^5$ of vibration cycles.

Barrat and Trizac [13] have recently considered one of the systems studied in the present paper. However, our treatment presents some differences:

- The bottom and top walls of [13] move in a sawtooth manner with a negligible excursion so that their positions are considered fixed, while our walls move sinusoidally with a non-negligible amplitude.
- The walls are not smooth in our treatment, but have a friction coefficient $\mu > 0$.
- The collisional models of our treatment and that of Barrat-Trizac are different (they do not distinguish between sticking and sliding collisions).
- We take into account gravity.

3 Results for a short system

The box dimensions were $L_x = 48\,d$ and $L_z = 32\,d$. Simulation runs were carried out using $N_1 = 150$ grains of each species. The static friction coefficient has been always chosen as $\mu = 0.1$. The stationary state is determined by the balance between the energy input provided by the vibrating walls at a frequency of 50 Hz and the dissipation due to inelastic collisions. The typical collision frequencies are of the order of $\nu_1 \sim 580$ Hz and $\nu_2 \sim 850$ Hz for the heavy

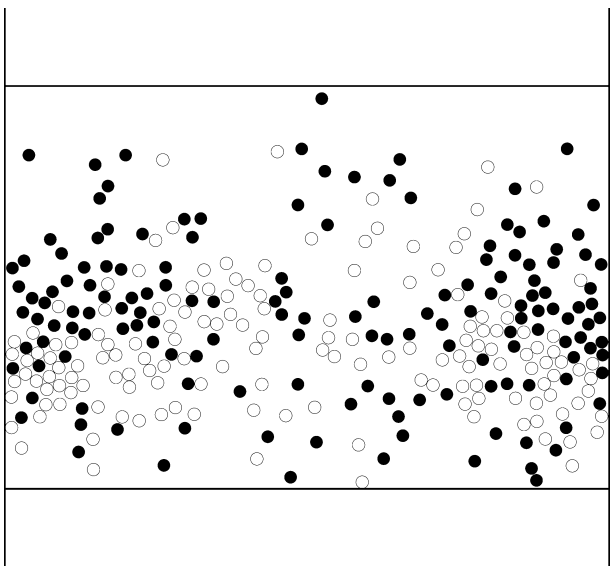

Fig. 1. Typical snapshot of the system described in section III. Open circles indicate particles of species 1, black circles particles of species 2

and light balls, respectively. A typical microscopic configuration of the system is shown in Fig. 1, where one sees that the container is more crowded near the center.

3.1 Temperature profiles

A first check of the model is represented by the analysis of the partial temperature profiles, two experimentally measured quantities.

The restitution coefficients were first set to $r_{11} = 0.93$ for 1-1 collisions, $r_{22} = 0.7$ for 2-2, and $r_{12} = 0.8$ for 1-2 collisions. This means that the more massive particles are also the more elastic ones. In Fig. 2 we show the partial translational temperature profiles for the two species, and observe that close to the vertical boundaries the two temperatures are essentially determined by the energy injected by the vibrating walls. Indeed, inter-particle collisions are rare within this region, and play no significant role because of the low local density (see Fig. 5). In addition, grains 1 and 2 impinging with the same speed on the mobile wall bounce with the same velocity ($V \propto A\omega$), hence the local value of the temperature ratio, $\gamma = T_2/T_1$ near the vibrating walls, turns out to be approximately $\gamma \sim m_1/m_2$, as shown in Fig. 2.

On the other hand, the temperature drops as the distance from the walls increases, while the ratio γ grows up to a plateau value, indicating that collisions tend to cool the mixture and render the two partial temperatures closer. Figure 2 clearly displays the breakdown of the kinetic energy equipartition already noticed in previous experimental and theoretical studies. The temperature ratio and the shape of temperature profiles agree with the ones measured by Feitosa and Menon [5], in particular the comparison between the top frame of our Fig. 2 and Fig. 3 of [5] is striking.

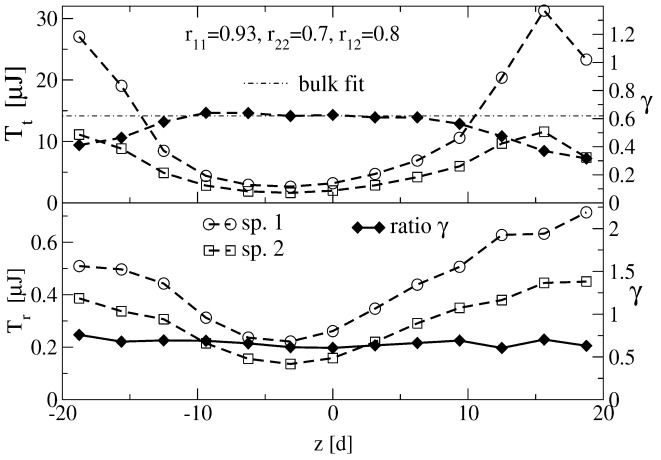

Fig. 2. Top panel: Translational temperature profiles for species 1 (circles) and species 2 (squares) for a mass ratio $m_1/m_2 = 3.03$, expressed in μJ (left scale), and temperature ratio (diamonds) T_2/T_1 (right scale). The vertical position is measured in particle diameters (d) relative to the geometric center of the cell. Bottom panel: rotational temperature profiles for species 1 (circles) and species 2 (squares) and temperature ratio T_2/T_1 (diamonds)

We also measured the rotational temperature profiles, shown in Fig. 2. We observe for rotational temperatures the same kind of equipartition breakdown that holds for translational degrees of freedom. Moreover, the absolute values of rotational and translational temperatures are quite different, as already reported by Luding [18] for a one-component, vibrated granulate. On the other hand, the ratio of the two rotational temperature profiles seems to be quite close to that of the translational temperature profiles.

For the sake of comparison we drew the ratio predicted by the theory of Barrat and Trizac [11] (formula (14) of their paper, called "bulk prediction" in the labels of our graphics) obtained by neglecting the rotations and assuming an homogeneous heating. The value predicted by the theory results independent of the driving intensity and is in very good agreement with the outcomes of the numerical simulations in the central ("bulk", i.e. far from the top and bottom boundaries) region.

We also modified the normal restitution coefficient between the horizontal walls and the heavy species (setting its value to 0.4) and studied how the temperature ratio was affected. This was done to modify the ratio T_2/T_1 near the walls. We discovered that the temperature ratio in the central region did not change significantly.

Interestingly Fig. 3 shows that, as the driving parameter Γ increases (increasing the frequency of the vibration ω), the plateau of the temperature ratio saturates around a value (about 0.63, in agreement with the value predicted in [11]). However, for smaller values of Γ, gravity becomes more relevant so that the spatial arrangement of the particles changes from that of a uniform gas to a more clusterized state. In fact, the plateau of T_2/T_1 disappears due to the fact that the average height of the center of mass decreases.

In Fig. 4, we changed the restitution coefficients and set $r_{11} = 0.7$, $r_{22} = 0.93$ for 2-2, and $r_{12} = 0.81$. Therefore now the more massive particles are the more inelastic.

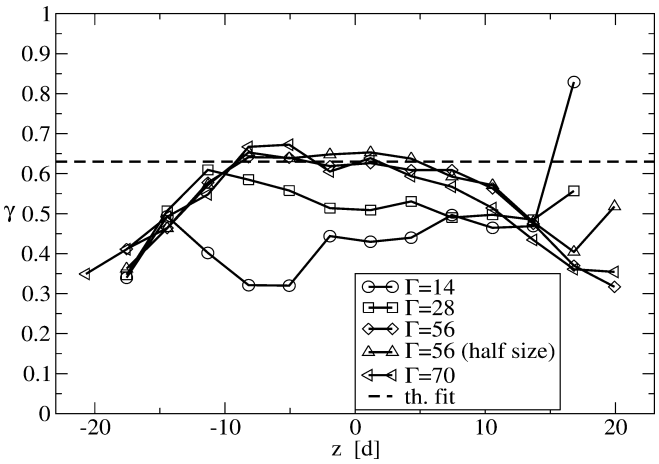

Fig. 3. Temperature ratio T_2/T_1 profiles obtained for different values of the driving parameter Γ (obtained changing the vibration frequency ω). The particle properties are the same as those of Fig. 2 and the number of each species is $N = 150$, apart the upper triangles, which refer to a system containing 75 particles of each species

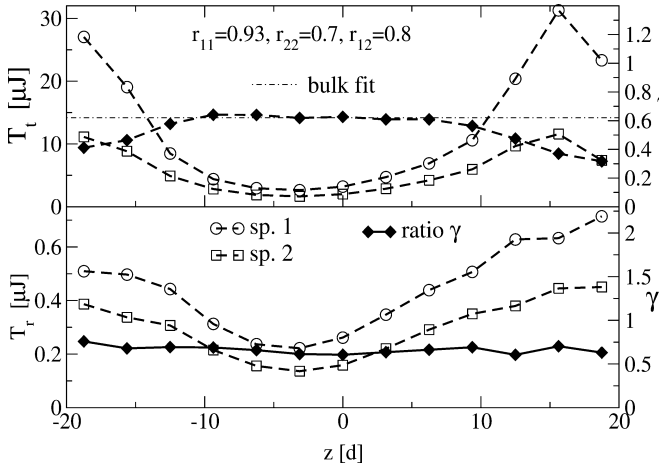

Fig. 4. Same as in Fig. 2, but with different restitution coefficients

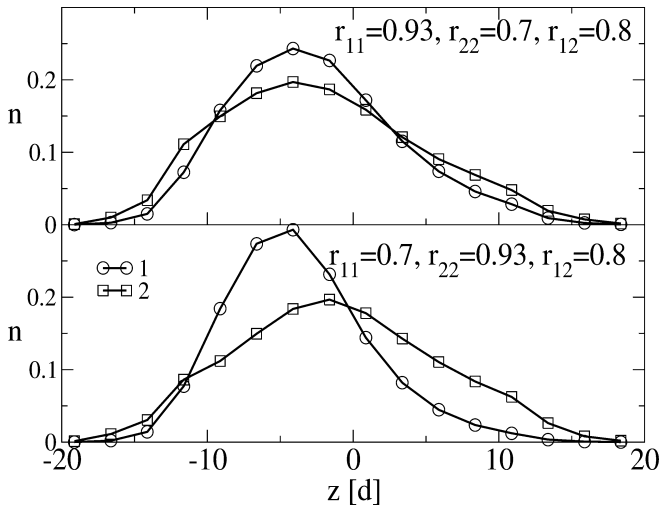

Fig. 5. Area fraction profiles n_1 and n_2. Control parameters are the same as in Fig. 1

We observe that, whereas the temperature profiles near the vibrating planes are nearly unchanged, because collisions are rare, the value of the temperature of the heavier species is lower and the temperature ratio is closer to 1. In this case the larger inelasticity of the heavier particles competes with the mass asymmetry which instead tends to make T_2/T_1 smaller. Again the comparison with the theory of Trizac and Barrat [11] is quite good.

3.2 Area fraction profiles

A second comparison of the theory with the experimental results is represented by the analysis of the area fraction profiles (see Fig. 5).

Due to the large value of the parameter Γ, the partial density profiles tend to be rather symmetric, with a maximum near the center. We also notice small differences in the density profiles, which reveal that the heavier species has higher concentration close to the center of the cell, while the lighter species is more spread.

Comparing the present results for the area fraction profiles with those recently obtained by employing a Direct Simulation Monte Carlo technique [12], we notice that the agreement is only qualitative, whereas the temperature ratios are in significantly better agreement.

We verified that removing tangential friction (coupling the translational and rotational degrees of freedom) does not change significantly the above scenario. In fact, the translational temperature and density profiles of the cases $\mu = 0$ and $\mu = 0.1$ show only small quantitative differences, more pronounced close to the horizontal walls.

3.3 Transversal profiles

We also studied the density and temperature profiles along the horizontal direction. To the best of out knowledge, no such measure has been reported in experimental works. In spite of the fact that the number of particles employed is not large, the stationarity of the system, allows to perform meaningful averages.

In Figs. 6 and 7 we observe that temperature profiles vanish close to side walls, while density profiles display their maxima in the same region. In order to gain further insight, we analyzed a sequence of snapshots of the dynamics, and observed that the system bears a denser cloud of grains in the vicinity of one of the side walls. Such a configuration was maintained over an interval of time much longer than the vibration period $2\pi/\omega$.

The cluster eventually "evaporates" to form again close to a randomly selected side wall. Over several periods of oscillation of the cell, we noticed an effective horizontal symmetry breaking, i.e. the number of particles in the right-hand and left-hand sides of the cell were rather different. The system is unstable with respect to horizontal density fluctuations and clusterizes spontaneously, until the vibrating bases wash out the cluster.

Moreover, we also observed some spontaneous tendency of the system to segregate the species, a fact which

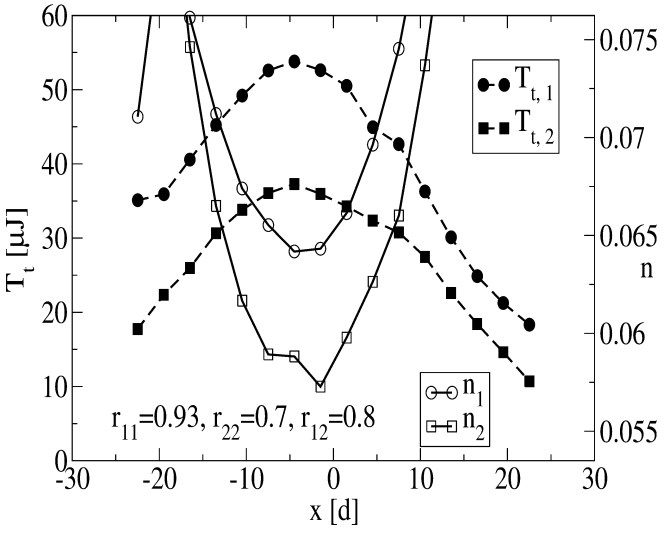

Fig. 6. Temperature profiles T_1 e T_2 (left scale) along the horizontal direction and area fractions n_1 and n_2 (right scale). Control parameters are the same as in Fig. 1

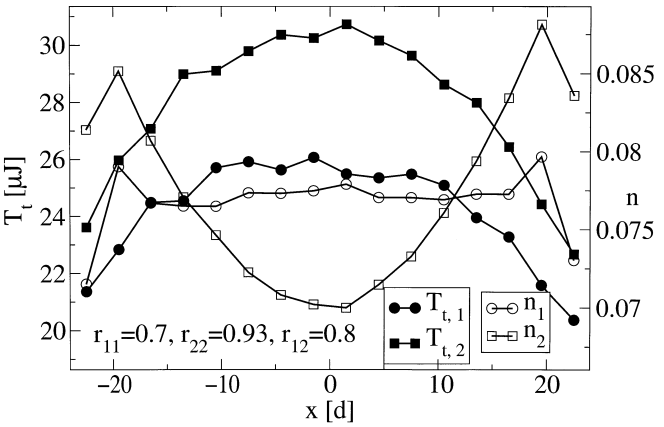

Fig. 7. Same as in Fig. 6, but with different restitution coefficients

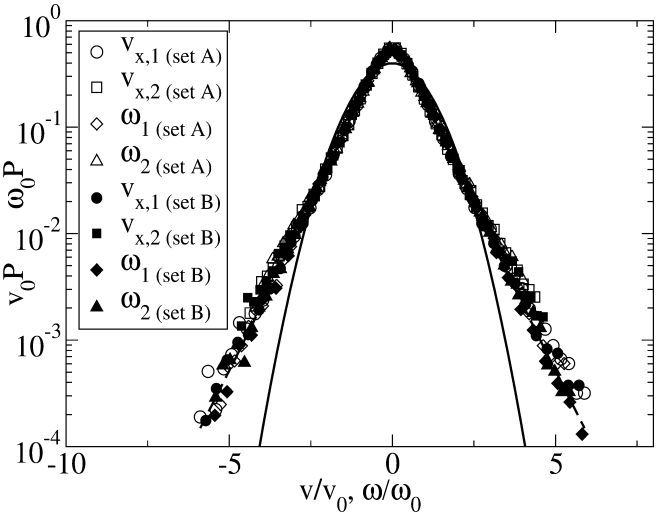

Fig. 8. Rescaled velocity distribution functions $< c > P(c) = f(c/ < c >)$ for translational velocities and angular velocities of both species. Set A corresponds to parameters of Fig. 2, set B to parameters of Fig. 3. The independent variables (v, ω) were rescaled by their mean squared value (v_0, ω_0). On rescaling, the distributions collapse nicely onto each other. The dashed curve is the fitting law discussed in the text, the continuous line is the Gaussian plotted as a reference for the eye

becomes more apparent at high densities. Both phenomena have their origin in the inelasticity. A possible qualitative explanation of the observed dynamics is as follows: particles with smaller restitution coefficient tend to group together, since the more energy they dissipate through 2-2 collisions, the denser the segregated domain becomes. Particles with higher restitution coefficient bounce for a longer time after a collision, and dilate more quickly.

3.4 Velocity probability distributions

We now illustrate how the inhomogeneity of the system affects the distribution of the velocities $P(v)$ in the transversal direction. As shown by recent work of [22,21] the velocity distribution function of vibrated granular gases is strongly non universal. It depends on several factors such as the number of monolayers, the nature of the granular fluid and the driving mechanism. For large drivings and nearly elastic particles ($r_{ij} = 0.96$) we observed that the distributions are nearly Gaussian and the density is uniform. As we increase the inelasticity the distribution function exhibits non Gaussian high velocity tails. Brey and coworkers found recently that $P(v)$ cannot be described by a simple stretched exponential $\exp(-(v/v_0)^\alpha)$ with a single value of α over the whole velocity range. Only the tails seem to be fitted by values of α in the interval between 1.5 and 2. In the present case we find tail exponents α even smaller than those found by Brey and Montero.

Figure 8 shows the distributions functions for the translational velocities along the horizontal direction. For sake of comparison, all the velocities were rescaled by their mean square values. We notice that the two transversal velocity distribution functions deviate from a Gaussian and are fitted by $f(c) = A/(\exp(\beta c^\alpha) + \exp(-\beta c^\alpha))$, with: $A = 1.068$, $\beta = 1.74$, $\alpha = 0.918$.

The exponential tails appear to have a smaller slope α than the theoretically predicted 3/2 value, for a uniform system stochastically driven [23]. This is consistent with the experimental results of Blair and Kudrolli [25]: when the number of monolayers is comparable to ours (about 5) and the system is rather inelastic, their velocity distributions have tails much fatter than $\exp(-c^{3/2})$.

The reason for the low value of the α exponent in our case is probably the fact that the effective restitution coefficient of the mixture is lower than that employed by Brey and Montero in their numerical investigation. This in turn determines a partial clusterization along the transversal direction with a consequent deviation from the gaseous state.

Figure 8 also shows the angular velocity distributions (rescaled by their mean square value, see caption). The angular velocity distributions can also be described by the same scaling function we used for translational velocity distributions.

3.5 Collision time distribution

Recently, Blair and Kudrolli utilizing high speed digital photography measured the collision statistics of grains bound to move on an inclined plane [24]. They determined the distribution of path lengths, $P(l)$ and showed that it deviates from the theoretical prediction for elastic hard spheres. In particular, $P(l)$ shows a peak in the small l region, not present in elastic systems. In order to assess the existence of such a behavior in the IHS model we performed similar measurements. Figure 9 displays the results for the collision times of the two species. One clearly sees that the probability density that a particle suffers a collision in a short interval is enhanced with respect to the elastic case. The physical reason for that lies in the existence of strong correlations which lead to the presence of clusters where the path lengths are shorter than in a uniform system. For the sake of comparison we plotted in Fig. 9 also the corresponding distribution of an elastic gas having the same density and granular temperature

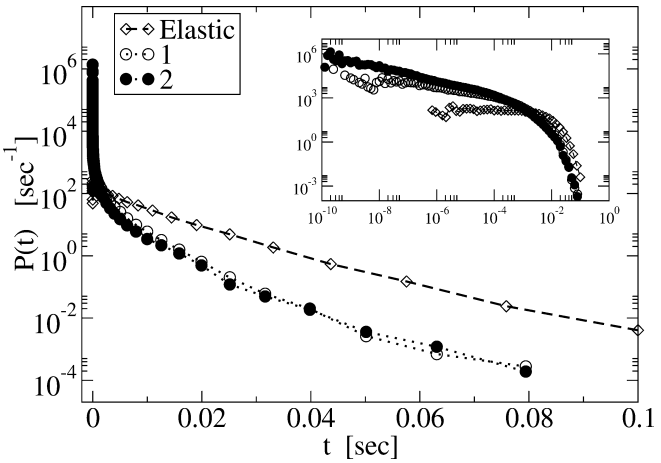

Fig. 9. Probability distribution functions of the collision times for the two components (system with $r_{11} = 0.93$, $r_{22} = 0.7$, $r_{12} = 0.8$). For comparison we plotted the corresponding distributions for an elastic system. The inset shows the same curves in log-log scale

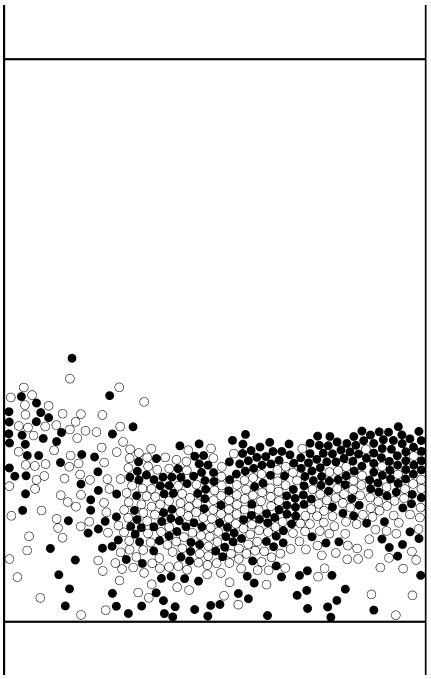

Fig. 10. Snapshot of the system described in IV. Open circles indicate particles of species 1, black circles particles of species 2

of our inelastic mixture. The effect of the shorter average collision time is clearly visible. We also notice that the ratio of the collision frequencies is approximately equal to the the ratio of the average velocities, as expected from elementary kinetic arguments.

4
Effect of a larger number of monolayers

When the number of monolayers (i.e. $N\,d/L_x$) increases one expects that the effect of gravity is more evident, resulting in a stronger inhomogeneity and asymmetry

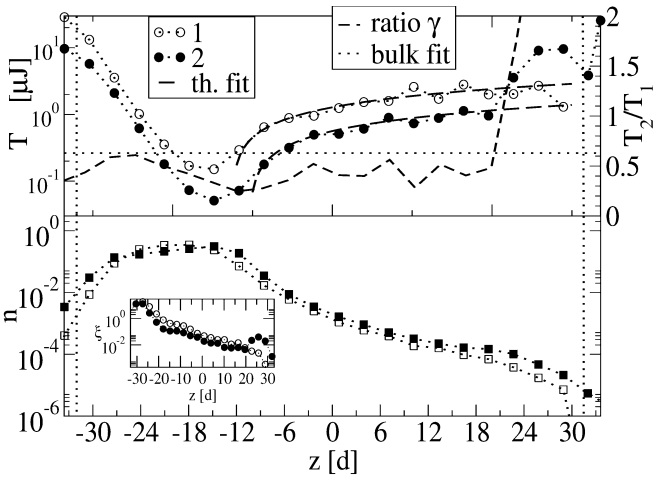

Fig. 11. Temperature and area fraction profiles for the system discussed in section IV. In the inset the dissipation rate $\xi(z)$ is shown. In the figure we compared our result against the hydrodynamic prediction $T \sim z^{3/2}$ (solid lines). The vertical dotted lines correspond to the rest position of the horizontal boundaries

of the system. We verified this scenario with a different numerical experiment: we took into account a box of dimensions $L_x = 48\,d$ and $L_z = 64\,d$ with 300 grains of each species ($r_{11} = 0.93$ for 1-1 collisions, $r_{22} = 0.7$ for 2-2, and $r_{12} = 0.8$ for 1-2 collisions, mass ratio $m_1/m_2 = 3.03$). A configuration of such system is shown in Fig. 10. The partial temperature profiles and density profiles are shown in Fig. 11. Now, the density and temperatures profiles are not symmetric with respect to the vertical direction. Most of the particles remain suspended above the bottom wall and are hit by those which are between the bottom wall and the bulk. Very few particles reach the upper vibrating wall, so that the granular temperature of the system is much lower at the top than at the bottom. One sees that near the lower vibrating wall the temperature profiles are similar to those of the shorter system, whereas in the bulk they are appreciably different. The average ratio is lower than in the $L_z = 32$ d case. An interesting feature present in Fig.11 is the presence of a region of increasing temperatures. Such a phenomenon has been predicted by the hydrodynamic theory of Brey et al. [3]. The theory predicts a temperature varying as $T \sim z^{3/2}$ in the region above the minimum. Such a prediction is verified by our simulation results.

Physically, the increase is due to the competition between the energy input from the walls and the small dissipation due to the reduced number of collisions associated with the low density region. This can be appreciated in the inset of figure 11 where the quantity $\xi(z) = n(z)T(z)^{3/2}$ is shown: $\xi(z)$ is proportional to the energy dissipation due to inelastic collisions among particles, being the collision rate $\propto nT^{1/2}$ and the average dissipated energy in a single collision $\propto T$. The graph of $\xi(z)$ reveals that the energy dissipation is much more relevant in the bottom region than in the middle and upper regions.

Correspondingly the velocity probability distribution functions (pdf) show an interesting behavior (see Fig. 12).

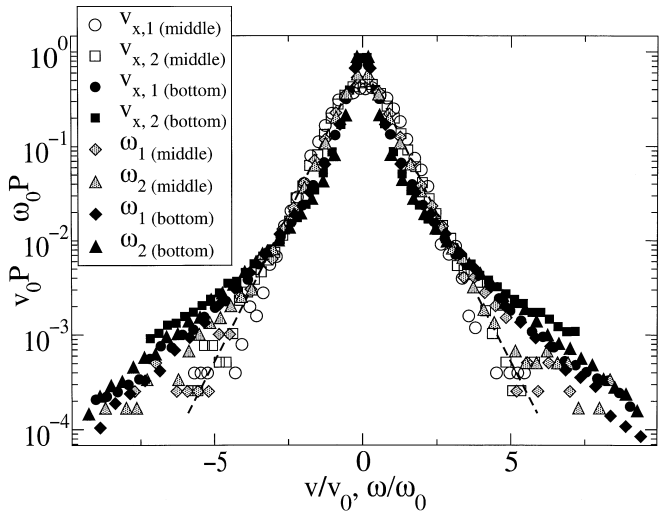

Fig. 12. Rescaled velocity distribution functions for the 48 × 64 system measured at different heights: the system has been divided into three regions of width L_x and height $L_y/3$ and the distributions of the translational and rotational velocities of the grains in the bottom and middle regions have been calculated

In fact, the shape of the rescaled pdf becomes narrower with the height. In the central region the measured pdf resemble the exponential shape measured in the short system (Fig. 8), whereas in the bottom region the pdf have more extended tails. Such a lack of universality was noted experimentally by Blair and Kudrolli [25], where velocity pdf's very similar to the ones shown in Fig. 8 have been obtained. The lack of universality was also noticed in [17]: there it was shown that the tails of the pdf became broader when the dissipation rate was increased. Here the mechanism is similar: the broader pdf are those measured in the bottom region, where the dissipation rate is higher.

5 Conclusions

Summarizing, we studied a systems of inelastic particles in vertically vibrated containers and subject to the gravitational field. The system was numerically investigated by using an Event-Driven dynamics. Firstly, our numerical simulation allows to test whether the modelization of the granular mixture along the line proposed by Walton [14] together with a realistic description of the moving plates is sufficient to reproduce the experimental results. The comparison is important because many theoretical approaches so far have neglected the finite displacement of the plates or assumed a saw-tooth law.

We also examined two similar setups which differ only for the aspect ratio of the container and for the number of particles. In the shorter system we determined the partial granular temperatures, their ratio, and the area fraction profiles along the vertical direction. Those measures are in very good qualitative agreement with the experimental results in [5], while a quantitative comparison requires a more detailed knowledge of the experimental parameters. Physically the lack of energy equipartition is determined by the different dissipation rates of the two components. Moreover, the way the energy is supplied by the walls to the two components determines together with the inelasticity parameters the actual value of the temperature ratio.

We also observed that density profiles are non-uniform along the horizontal direction, as well, indicating that the particles tend to clusterize in the vicinity of side walls.

Interestingly, the distributions of the translational and rotational velocities collapse onto each other, under proper rescaling. The scaling function displays a stretched exponential behavior. In the case of larger aspect ratio we observed that pdf referring to different heights fail to collapse.

Finally the distribution of flight times between successive collisions has been measured and compared to that of an elastic system: the inelasticity has the effect of enhancing the statistics of very short times.

In the taller system we have again obtained the temperature and area fraction profiles, observing a stronger inhomogeneity and asymmetry. In this case the area fraction is much larger near the bottom wall, reaching higher values than in the previous experiment. The middle-upper region seems to be qualitatively well described by recent hydrodynamic theories developed for one component systems. Here the velocity pdf's display a non-universal behavior, with broader tails in the more dense (and dissipative) regions that are in fair qualitative agreement with the ones obtained in [25].

6 Appendix

In order to make it simpler for the reader to interpret the present model, we present an appendix in which we explicitly state the collision rules [26].

The colliding particles are characterized by radii R_1 and R_2, positions $\mathbf{r}_1$ and $\mathbf{r}_2$, translational velocities $\mathbf{v}_1$ and $\mathbf{v}_2$ and rotational (angular) velocities $\boldsymbol{\omega}_1$ and $\boldsymbol{\omega}_2$ (we assume that if $\boldsymbol{\omega}$ is parallel and in the direction of the z axis, than the rotation is anticlockwise if seen from above the xy plane). We introduce the normal unitary vector joining the centers of the particles $\mathbf{n} = (\mathbf{r}_2 - \mathbf{r}_1)/|\mathbf{r}_2 - \mathbf{r}_1|$ and the tangential unitary vector $\mathbf{t}$ obtained rotating $\mathbf{n}$ by an anti-clockwise angle $\pi/2$. Then we introduce the relative velocity $\mathbf{g}$, the velocity of the center of mass $\mathbf{V}$ and the velocities of the particles in the center of mass frame $\boldsymbol{\zeta}_1$ and $\boldsymbol{\zeta}_2$:

$$\mathbf{g} = \mathbf{v}_1 - \mathbf{v}_2 \tag{2a}$$

$$\mathbf{V} = \frac{m_1\mathbf{v}_1 + m_2\mathbf{V}_2}{m_1 + m2} \tag{2b}$$

$$\boldsymbol{\zeta}_1 = \frac{m_{eff}}{m_1}\mathbf{g} \tag{2c}$$

$$\boldsymbol{\zeta}_2 = -\frac{m_{eff}}{m_2}\mathbf{g} \tag{2d}$$

where $m_{eff} = m_1 m_2/(m_1 + m_2)$.

Then we decompose the relative velocity $\mathbf{g}$ on the orthonormal basis given $\mathbf{n}$ and $\mathbf{t}$, as well as the velocities of the particles in the center of mass frame, i.e.:

$$g_n = (\mathbf{v_1} - \mathbf{v_2}) \cdot \mathbf{n} \tag{3a}$$
$$g_t = (\mathbf{v_1} - \mathbf{v_2}) \cdot \mathbf{t} \tag{3b}$$
$$\zeta_{n\beta} = \frac{m_{eff}}{m_\beta} g_n \tag{3c}$$
$$\zeta_{t\beta} = \frac{m_{eff}}{m_\beta} g_t \tag{3d}$$

with $\beta = 1, 2$ the index of the particle.

We finally introduce g_c as the relative circular velocity at the point of contact and g_r as the total tangential relative velocity (circular and translational) at the point of contact:

$$g_c = R_1\omega_1 + R_2\omega_2 \tag{4a}$$
$$g_r = g_c + g_t \tag{4b}$$

To characterize the collision rules we use a model that take into account a reduction of normal relative velocity (g_n), a reduction of total tangential relative velocity (g_r) and an exchange of energy between those two degrees of freedom. The reduction of normal relative velocity is modeled as usual by means of a restitution coefficient $\alpha \in [0, 1]$:

$$g'_n = -\alpha g_n. \tag{5}$$

We assume a dependence of α by the relative velocity of the form:

$$\alpha(g_n) = \begin{cases} 1 - (1 - \alpha_0)\frac{|g_n|}{v_0}^{\frac{3}{4}} & \text{per } \; g_n < v_0 \\ \alpha_0 & \text{per } \; g_n > v_0 \end{cases}$$

where α_0 is a constant which stands for r_{ij}, $v_0 = \sqrt{gD}$, with D the average diameter of the particles (and g is the gravity acceleration). From equations (5) we obtain the update of normal velocities in the center of mass frame:

$$\zeta'_{n1} = -\alpha \frac{m_{eff}}{m_1} g_n \tag{6a}$$
$$\zeta'_{n2} = \alpha \frac{m_{eff}}{m_2} g_n$$

What lacks now is an expression for the tangential and angular velocities after the collisions. We distinguish between two possible cases: sliding or sticking collisions. The condition that allows to determine if a collision is sticking or sliding is the following:

$$\frac{|g_r|}{g_n} \geq \frac{l+1}{l}\mu(1+\alpha) \tag{7}$$

where l is the non-non-dimensionalized inertia moment and is equal to $1/2$ or $2/5$ if the particle is a disk or a sphere respectively, while μ is the static friction coefficient of the surface of the particles which in the following will be assumed to be equal to the dynamic friction coefficient.

In the sliding case we use the following rules to update the tangential components of the velocities of the particles in the center of mass frame:

$$\zeta'_{t1} = \zeta_{t1} - \mu(1+\alpha)\frac{m_{eff}}{m_1} g_n sign(g_r) \tag{8a}$$
$$\zeta'_{t2} = \zeta_{t2} + \mu(1+\alpha)\frac{m_{eff}}{m_2} g_n sign(g_r) \tag{8b}$$
$$R_1\omega'_1 = R_1\omega_1 - \frac{\mu(1+\alpha)}{l}\frac{m_{eff}}{m_1} g_n sign(g_r) \tag{8c}$$
$$R_2\omega'_2 = R_2\omega_2 - \frac{\mu(1+\alpha)}{l}\frac{m_{eff}}{m_2} g_n sign(g_r) \tag{8d}$$

In the case of a sticking collision, instead, the update rules are obtained considering that:

$$\zeta'_{t1} - \zeta'_{t2} + R_1\omega'_1 + R_2\omega'_2 = 0 \tag{9}$$

from which, after calculations, one gets:

$$\zeta'_{t1} = \frac{1}{l+1}\zeta_{t1} - \frac{l}{l+1}\frac{m_{eff}}{m_1}(R_1\omega_1 + R_2\omega_2) \tag{10a}$$
$$\zeta'_{t2} = \frac{1}{l+1}\zeta_{t2} + \frac{l}{l+1}\frac{m_{eff}}{m_2}(R_1\omega_1 + R_2\omega_2) \tag{10b}$$
$$R_1\omega'_1 = R_1\omega 1\left[\frac{l}{l+1} + \frac{m_{eff}}{(l+1)m_2}\right] \tag{10c}$$
$$- R_2\omega_2\frac{m_{eff}}{(l+1)m_1} - \frac{1}{l+1}\zeta_{t1} \tag{10d}$$
$$R_2\omega'_2 = R_2\omega 2\left[\frac{l}{l+1} + \frac{m_{eff}}{(l+1)m_1}\right] \tag{10e}$$
$$- R_1\omega_1\frac{m_{eff}}{(l+1)m_2} + \frac{1}{l+1}\zeta_{t2} \tag{10f}$$

The velocity of particles in the absolute frame are finally obtained in the two cases (considering that the center of mass is not perturbed by the collision) by the equation:

$$\mathbf{v}'_\beta = \mathbf{V} + \zeta'_{n\beta}\mathbf{n} + \zeta'_{t\beta}\mathbf{t} \tag{11}$$

(for particle of index β) leading to the following global collision rule for translational velocities:

$$\mathbf{v}'_1 = \mathbf{v}_1 - (1+\alpha)\frac{m_2}{m_1+m_2}[(\mathbf{v}_1 - \mathbf{v}_2)\cdot\mathbf{n}]\mathbf{n} - \begin{cases} sign(g_r)\mu(1+\alpha)\frac{m_2}{m_1+m_2}[(\mathbf{v}_1 - \mathbf{v}_2)\cdot\mathbf{n}]\mathbf{t} \text{ (sliding)} \\ \frac{m_1 - lm_2}{(l+1)(m_1+m_2)}[(\mathbf{v}_1 - \mathbf{v}_2)\cdot\mathbf{t}]\mathbf{t} \\ \quad -\frac{l}{l+1}\frac{m_2}{m_1+m_2}(R_1\omega_1 + R_2\omega_2) \text{ (stick)} \end{cases} \tag{12a}$$

$$\mathbf{v}'_2 = \mathbf{v}_2 + (1+\alpha)\frac{m_1}{m_1+m_2}[(\mathbf{v}_1 - \mathbf{v}_2)\cdot\mathbf{n}]\mathbf{n} + \begin{cases} sign(g_r)\mu(1+\alpha)\frac{m_1}{m_1+m_2}[(\mathbf{v}_1 - \mathbf{v}_2)\cdot\mathbf{n}]\mathbf{t} \text{ (sliding)} \\ \frac{m_2 - lm_1}{(l+1)(m_1+m_2)}[(\mathbf{v}_1 - \mathbf{v}_2)\cdot\mathbf{t}]\mathbf{t} \\ \quad +\frac{l}{l+1}\frac{m_1}{m_1+m_2}(R_1\omega_1 + R_2\omega_2) \text{ (stick)} \end{cases} \tag{12b}$$

while for rotational velocities:

$$R_1\omega_1' = \begin{cases} R_1\omega_1 - \frac{\mu(1+\alpha)}{l}\frac{m_2}{m_1+m_2}g_n sign(g_r) \text{ (stick)} \\ R_1\omega 1\left[\frac{l}{l+1} + \frac{m_1}{(l+1)(m_1+m_2)}\right] \\ -R_2\omega_2\frac{m_2}{(l+1)(m_1+m_2)} - \frac{1}{l+1}\zeta_{t1} \text{ (slide)} \end{cases} \quad (13a)$$

$$R_2\omega_2' = \begin{cases} R_2\omega_2 - \frac{\mu(1+\alpha)}{l}\frac{m_1}{m_1+m_2}g_n sign(g_r) \text{ (stick)} \\ R_2\omega_2\left[\frac{l}{l+1} + \frac{m_2}{(l+1)(m_1+m_2)}\right] \\ -R_1\omega_1\frac{m_1}{(l+1)(m_1+m_2)} + \frac{1}{l+1}\zeta_{t1} \text{ (slide)} \end{cases} \quad (13b)$$

References

1. H. M. Jaeger, S. R. Nagel & R. P. Behringer, Rev. Mod. Phys. 68 (1996), p. 1259
2. I. Goldhirsch & G. Zanetti, Phys. Rev. Lett. 70 (1993), p. 1619
3. J. J. Brey, M. J. Ruiz-Montero, F. Moreno & R. Garcia-Rojo, Phys. Rev. E 65 (2002), p. 061302
4. A. Baldassarri, U. Marini Bettolo Marconi & A. Puglisi, Phys. Rev. E 65 (2002), p. 051301
5. K. Feitosa e N. Menon, Phys. Rev. Lett. 88 (2002), p. 198301
6. R. D. Wildman & D. J. Parker, Phys. Rev. Lett. 88 (2002), p. 064301
7. S. R. Dahl, C. M. Hrenya, V. Garzó e & J. W. Dufty, 2002, Phys. Rev. E 66 (2002), p. 041301
8. Vicente Garzó e, & James Dufty, Phys. Rev. E 60 (1999), p. 5706
9. U. Marini Bettolo Marconi & A. Puglisi, Phys. Rev. E 65 (2002), p. 051305
10. U. Marini, Bettolo Marconi & A. Puglisi, Phys. Rev. E 66 (2002), p. 011301
11. Alain Barrat e Emmanuel Trizac, Granular Matter 4 (2002), p. 57
12. A. Pagnani, U. Marini Bettolo Marconi, & A. Puglisi, Phys. Rev. E 66 (2002), p. 051304
13. A. Barrat e E. Trizac, Phys. Rev. E 66 (2002), p. 051303
14. O. R. Walton, Particulate Two-Phase Flow, M.C. Roco editor, Butterworth-Heinemann, Boston (1993), p. 884
15. C. Bizon, M. D. Shattuck, J. B. Swift & H. Swinney, Phys. Rev. E 60 (1999), p. 4340
16. C. Cattuto, submitted to Computers in Science and Engineering
17. A. Puglisi, V. Loreto, U. Marini Bettolo Marconi, A. Petri & A. Vulpiani, 1998 Phys. Rev. Lett. 81, 3848 and Phys. Rev. E 59 (1999), p. 5582
18. S. McNamara & S.Luding, Phys. Rev. E 58 (1998), p. 2247
19. We verified that, assuming a sawtooth time dependence of the position of the vibrating walls (instead of a sinusoidal one), the velocity p.d.f did not change appreciably
20. A. Baldassarri, U. Marini Bettolo Marconi, A. Puglisi, & A. Vulpiani, Phys. Rev. E 64 (2001), p. 011301
21. J. Javier Brey & M. J. Ruiz-Montero, 2002, cond-mat/0210158
22. J. S. van Zon & F. C. MacKintosh, 2002, cond-mat/0205512
23. T. P. C. van Noije & M. H. Ernst, Granular Matter 1 (1998), p. 57
24. D. L. Blair & A. Kudrolli, private communication
25. D. L. Blair & A. Kudrolli, Phys. Rev. E 64 (2001), p. 050301
26. Z. Farkas, P. Tegzes, A. Vukics, T. Vicsek, cond-mat/9905094 version 7/5/1999